Noname manuscript No.
(will be inserted by the editor)

OMA Analysis of a launcher under operational conditions with time-varying properties

M. Eugeni · G. Coppotelli
F. Mastroddi · P. Gaudenzi · S. Muller
B. Troclet

Received: date / Accepted: date

Abstract The objective of the paper is the investigation of the capability of Operational Modal Analysis approaches to deal with time-varying system in the low-frequency domain. Specifically, the problem of the identification of the dynamic properties of a launch-vehicle, working under actual operative conditions, is studied. Two OMA methods are considered: the Frequency Domain Decomposition and the Hilbert Transform Method. It is demonstrated that both OMA approaches allow the time-tracking of modal parameters, namely, natural frequencies, damping ratios and mode shapes, from the response accelerations only recorded during actual flight tests of a launcher characterized by a large mass variation due to fuel burning typical of the first phase of the flight.

Keywords Operational Modal Analysis · Output Only · Launchers · Launch systems · Dynamical Identification · Time-Varying systems

M. Eugeni, G. Coppotelli, F. Mastroddi, P. Gaudenzi
Department of Mechanical and Aerospace Engineering
University of Rome *"La Sapienza"*
via Eudossiana, 18, 00184 Rome - Italy
E-mail: marco.eugeni@uniroma1.it

S. Muller
Expert in Structural Analysis,
Airbus Defence and Space, Les Mureaux, France

B. Troclet
Senior Expert in Structural Analysis,
Airbus Defence and Space, Les Mureaux, France
Half time Professor,
ENS Cachan/Université Paris Saclay, Frace

1 Introduction

The development of Operational Modal Analysis (OMA) methods allows estimating the modal parameters of a structure by using vibration responses only. Thus, OMA methodologies are of great importance from the industrial point of view. Indeed, such methods permit to evaluate the behavior of a structural system under its operative conditions considering its actual boundary conditions and excitation levels, see Ref. [1]. Several techniques, both in frequency and in time domain, have been developed in recent years. Among the OMA methods, it is worth recalling the Frequency Domain Decomposition, FDD, the Hilbert Transform Method, HTM, and the Balanced Realization, BR, approach, see Refs. [2,3,4,5]. In the FDD method, the natural frequencies and mode shapes are gained from the evaluation of the frequency-dependent spectral characteristics of the output Power Spectral Density (PSD) matrix through the Singular Value Decomposition transformation technique. On the other hand the Hilbert Transform Method enables the estimate of the biased Frequency Response Functions, FRF's,directly from the output PSD spectra by taking advantages of the properties of the Hilbert transform applied to causal signals (Ref. [6]). From this biased FRFs the modal parameters are easily estimated by introducing residue-pole estimates available in literature. The Balanced Realization approach belongs to the Stochastic Subspace Identification methods, SSI, in which the state-space model is associated to the observed output responses through the so called orthogonal projection technique (Refs. [5] and [7]). In particular, the Balanced Realization, which works in the time domain, provides the observability matrix of the studied system starting from the so-called Hankel matrix built using the correlation functions evaluated from the output time responses [5]. The Stochastic Subspaces Identification can be performed also in the time domain with the so-called Frequency-Stochastic Subspaces Identification, f-SSI, which uses the same procedure of BR-SSI method but in the frequency domain computing the Vandermonde matrix with the output spectra [7].

In the present paper the identification in low frequency domain of a launcher vehicle by using data recorded during flight tests is considered. In particular, the identification is performed in terms of natural frequencies, damping ratios and variation of mode shapes. This important industrial application permits to consider some critical issues about the identification procedure via OMA methodologies. The analyzed system is characterized by time-dependency of its dynamical properties because its mass is varying due to the burning propellant. Thus, it has been necessary to determine a criterion of practical applicability of the OMA techniques for this kind of applications. This aspect is relevant in that all the identification OMA techniques are based on the assumption that the system intrinsic parameters like mass, stiffness and damping properties are constant in time and therefore, the intrinsic system signatures as its frequency response functions (FRF) keep their nature for any time-shift of the input/output recording. Unfortunately, because of these parameter variations (which is the typically mass variation of a launcher with solid or liquid

propeller), the result of a frequency domain analysis will give spectra that are dependent on the length of acquisition time window. Specifically, FRF obtained by FFT performed in a given time window will give a frequency-peak (resonance) with different locations because of the variations of mass quantity in the system. At limit, for a very long acquisition time, the resulting obtained FRF will average these behaviors and no information could be available on the variation of the frequency peak in time. On the other hand, the use of local and sufficiently short time windows to perform FFT could imply a frequency step for FRF function too large, namely, a frequency resolution, too coarse. Therefore, a quantitative evaluation of these effect and a rational choice for a compromise is presented in order to define the field of applicability of the time-invariant identification procedure. In Ref. [11] the problem of estimating the modal parameters of a luncher has been addressed even if without going into a detailed analysis of the critical aspect of this systems. As a further contribution the problem of uncertainties associated with the identification process has been addressed. This is a well-known issue related to dynamical identification and it has been deeply studied in literature, see Refs. [12,13,14, 15]. In the present paper, it will be analyzed from the point of view of system theory by studying how this uncertainties affect the poles of identified system. In particular, it has been demonstrated that the uncertainties associated to the identification process are determined by those associated to the natural frequencies evaluation.

The results here presented came from an activity developed by the Department of Mechanical and Aerospace Engineering of University of Roma *La Sapienza* and *Airbus Defence and Space*, a leading industry in the launcher sector. It is worth to remember that if, from one side, the considered study permits to evaluate the applicability of OMA methodologies to time-varying systems giving the possibility to address some theoretical aspects of operational modal analysis based identification process as already explained, on the other side, it gives the possibility to consider a practical application of clear interest for the aerospace industry. Indeed, the dynamic identification of a Launch Vehicle (LV) structure is of great importance for launcher industry because the availability of a validated mechanical model allows an accurate prediction of launcher dynamical performances thus reducing the time-to-market in developing phase, Ref. [16]. The vibrational data of launcher in its actual environmental conditions is an essential input necessary for the characterization of its dynamic behavior and, therefore, for updating the numerical models of the structure and for improving the design. Unfortunately, the operative costs for the experimental acquisition of such a data is often very expansive and the quality of acquired signal data is very coarse because of the difficult environmental conditions of the test. Another critical issue is specifically related to the standard procedures because, in the considered case, the system input load in the operative condition cannot be practically determined and only the output vibration level can be measured. Thus, the above aspects and limitations in the launcher vehicles dynamical evaluation make the OMA techniques of great practical interest for this kind of applications.

The dynamic identification of the launcher is provided by applying two different Operational Modal Analysis: the Fourier Domain Decomposition and the Hilbert Transform Method. Both methods has been demonstrated are able to track the time behavior of the natural frequencies, damping ratios and mode shapes of the studied launcher vehicle.

In Section 2 the used methodologies are presented in their theoretical aspects and in Sec. 3 a criterion of applicability of OMA techniques for time-varying systems is presented. Finally, in Sec. 4 the results of the analysis of two different flights cases are presented and in Sec. 5 some remarks about the accuracy of the estimated are given. In Sec. 6 some final comments are given.

2 Theoretical Background

Let us consider a linear system excited by a stochastic load representing the time evolution of a vibrating structure. Its Frequency Response Function (FRF) matrix, $\mathbf{H}(\omega) \in \mathcal{C}^{N_o \times N_i}$,can be expressed, by assuming N_m significant modes, as:

$$\mathbf{H}(\omega) = \mathbf{\Psi} \left[j\omega \mathbf{I} - \mathbf{\Lambda} \right]^{-1} \mathbf{\Phi}^T \tag{1}$$

where $\mathbf{\Psi} \in \mathcal{C}^{N_o \times N_m}$ is the mode shapes matrix evaluated in the N_o output degrees of freedom and $\mathbf{\Phi} \in \mathcal{C}^{N_i \times N_m}$ is the modal participation matrix evaluated in the N_i input degrees of freedom. The poles of the system, $\lambda_n = \lambda_{R_n} + j\lambda_{I_n},\ n = 1, \cdots, 2N_m;\ \ \lambda_{I_n} = \omega_n$, are the terms of the diagonal matrix $\mathbf{\Lambda}$ and contain the natural frequencies $f_n = \frac{\omega_{dn}}{2\pi}$ and the damping ratios $\zeta_n = -\frac{\lambda_{R_n}}{\lambda_{I_n}}$. As a result, the FRF matrix could be expressed in terms of the modal parameters as an expansion of partial fractions [8]:

$$\mathbf{H}(\omega) = \sum_{n=1}^{N_m} \left(\frac{\boldsymbol{\psi}^{(n)} \boldsymbol{\varphi}^{(n)T}}{j\omega - \lambda_n} + \frac{\boldsymbol{\psi}^{(n)*} \boldsymbol{\varphi}^{(n)H}}{j\omega - \lambda_n^*} \right) \tag{2}$$

The output spectral density function matrix, $\mathbf{G}_{yy}(\omega_k) \in \mathcal{C}^{N_o \times N_o},\ k = 1, \cdots, N_t/2$ can be built from the evaluation of the spectral density functions, $G_{y_i y_j}(\omega_k)$, defined between the i-th and j-th output responses as:

$$\mathbf{G}_{yy}(\omega_k) = \begin{pmatrix} G_{y_1 y_1}(\omega_k) & \dots & G_{y_1 y_{N_o}}(\omega_k) \\ \vdots & \ddots & \vdots \\ G_{y_{N_o} y_1}(\omega_k) & \dots & G_{y_{N_o} y_{N_o}}(\omega_k) \end{pmatrix} \tag{3}$$

Introducing, in a similar way, the input spectral density matrix defined between the N_i inputs, *i.e.*, $\mathbf{G}_{ff}(\omega_k) \in \mathcal{C}^{N_i \times N_i}$, their relationship through the FRF matrix of the system, $\mathbf{H}(\omega_k) \in \mathcal{C}^{N_o \times N_i}$, can be written as:

$$\mathbf{G}_{yy}(\omega_k) = \mathbf{H}(\omega_k) \mathbf{G}_{ff}(\omega_k) \mathbf{H}^H(\omega_k) \tag{4}$$

where the assumption of white noise input excitation implies that $\mathbf{G}_{ff}(\omega_k)$ is frequency independent, that is $\mathbf{G}_{ff}(\omega_k) = \mathbf{G}_{ff}$, where $\mathbf{G}_{ff}$ is a diagonal matrix when the input excitation is uncorrelated in the space domain. A combination of the Eqs.(4) and (2) yields the following expression that decomposes the output spectral density function matrix in the modal components:

$$\mathbf{G}_{yy}(\omega_k) = \sum_{i=1}^{N_m} \left(\frac{\boldsymbol{\psi}^{(i)} \bar{\boldsymbol{\varphi}}^{(i)T}}{j\omega_k - \lambda_i} + \frac{\boldsymbol{\psi}^{(i)*} \bar{\boldsymbol{\varphi}}^{(i)H}}{j\omega_k - \lambda_i^*} + \frac{\bar{\boldsymbol{\varphi}}^{(i)} \boldsymbol{\psi}^{(i)T}}{-j\omega_k - \lambda_i} + \frac{\bar{\boldsymbol{\varphi}}^{(i)*} \boldsymbol{\psi}^{(i)H}}{-j\omega_k - \lambda_i^*} \right) \quad (5)$$

in which $\bar{\boldsymbol{\varphi}}^{(i)}$ takes into account the contribution of the input excitation to the i-th participation factor. In the following subsection a brief recall of the methods considered in the paper is reported for the sake of completeness. More details could be found for each approach in the provided specific references.

2.1 Frequency Domain Decomposition

The FDD is based on the singular value decomposition of the response spectral matrix. In particular, being $\mathbf{G}_{yy}^H(\omega_k) = \mathbf{G}_{yy}(\omega_k)$, namely, a Hermitian matrix with real and positive diagonal elements, the singular value decomposition of the output spectral density matrix, for each of the k-th spectral lines can be decomposed as [2]:

$$\mathbf{G}_{yy}(\omega_k) = \mathbf{U}_k(\omega_k) \boldsymbol{\Sigma}_k(\omega_k) \mathbf{U}_k^H(\omega_k) \quad (6)$$

in which $\mathbf{U}_k(\omega_k) \in \mathcal{C}^{N_o \times N_o}$ is the matrix of left singular vectors and $\boldsymbol{\Sigma}_k(\omega_k) \in \mathcal{R}^{+(N_o \times N_o)}$ is the diagonal matrix of singular values. Under the hypothesis that the structure behaves as a single degree of freedom system around the peak of resonance, ω_n, then the rank of $\mathbf{G}_{yy}(\omega_k)$ is practically unitary (and then only one singular value will differ from zero) when the current frequency ω_k approaches one of the natural frequency of the structure, ω_n. In addition, by comparing Eq. (5) and Eq. (6) when $\omega_k = \omega_n$, a good estimate of the mode shape could be achieved from the singular vector corresponding to the only non-zero singular value. Moreover, taking an inverse Fourier transform of Eq.(5), the correlation matrix could be written in terms of the modal parameters as:

$$\mathbf{R}(\tau) = \sum_{i=1}^{N_m} \left(\boldsymbol{\psi}^{(i)} \bar{\boldsymbol{\varphi}}^{(i)} e^{\lambda_i \tau} + \boldsymbol{\psi}^{(i)*} \bar{\boldsymbol{\varphi}}^{(i)H} e^{\lambda_i^* \tau} \right) \quad (7)$$

If the mode shape are well separated and if such correlation functions are evaluated by inverse Fourier transforming the power spectral density matrix in the neighborhood of the identified natural frequency then they correspond to the free decay of an equivalent SDOF system so permitting the identification

of the damping ratio. Indeed, the logarithmic decrement technique could be applied to estimate the damping ratio [9,10]. In order to define the frequencies interval where the system behaves like a SDOF, the mode shape associated to the identified frequency is compared by using the Modal Assurance Criterion (MAC) with those associated with the neighboring frequencies. Thus, by fixing a critical value for the MAC, namely, the Threshold MAC, the searched interval is obtained and the damping ratio can be identified.

2.2 Hilbert Transform Method

The advantage in using the Hilbert transform is about the capability of estimating the imaginary part of the Fourier transform of a time causal function starting from the real part [6]. The Hilbert transform of a signal $x(t)$ is defined as the Cauchy principal value of

$$\hat{x}(t) = \mathcal{H}[x(t)] = \frac{1}{\pi} \int_{-\infty}^{+\infty} \frac{x(\tau)}{t-\tau} d\tau \tag{8}$$

The polar representation of a driving point FRF is given by

$$H_{ii}(\omega) = |H_{ii}(\omega)| e^{-j\phi_{ii}(\omega)} \tag{9}$$

or, by introducing the natural logarithm, could be expressed as

$$ln\left[H_{ii}(\omega)\right] = G_{ii}(\omega) - j\phi_{ii}(\omega) \tag{10}$$

in which $G_{ii}(\omega) = ln|H_{ii}(\omega)|$ is the gain function. Considering that the real part of the FRF is an even function and the imaginary part is an odd function, therefore the gain and the phase are even and odd, respectively. As a result the left-hand side of the Eq.(10) could be expressed as the sum of a pair of Hilbert transform functions:

$$\phi_{ii}(\omega) = -\hat{G}_{ii}(\omega) \tag{11}$$

The gain function is related to the spectral density function by Eq.(4), applying the natural logarithm and performing the Hilbert transform, it becomes:

$$\mathcal{H}\left[\ln(G_{y_i y_i}(\omega))\right] = 2\mathcal{H}\left[\ln|H_{ii}(\omega)|\right] \tag{12}$$

in which the input spectral density contribution, $G_{f_i f_i}$, is null, as the Hilbert transform of a constant is zero. Combining the previous Eqs.(11) and (12) it is possible to write

$$\phi_{ii}(\omega) = -\frac{1}{2}\mathcal{H}\left[\ln(G_{y_i y_i}(\omega))\right] \tag{13}$$

Therefore, the FRF in the i-th driving point is available. It is possible to demonstrate that the off-diagonal terms of the FRF are derivable from the comparison between the commonly used H1 and H2 estimators [3].

$$H_{ij}(\omega) = \frac{G_{y_i y_j}(\omega)}{\sqrt{G_{f_i f_i}} H^*_{ii}(\omega)} \tag{14}$$

Obviously the estimated functions are unbiased depending on the unknown input forces. The modal parameters are evaluated with a least square approximation, considering the expression of FRF in pole-residue terms, Eq.(2).

In the frequency range of definition of the FRF, the number of modes, N_m, is not known, therefore a stabilization diagram is introduced to estimate it by means of an iterative procedure. It is worth remarking that the structural properties are independent from the order used to describe the system, thus stable poles are representative of natural frequencies [10].

3 A criterion of applicability of OMA techniques for time-dependent systems

The OMA hypotheses require a linear time-independent system excited by a white noise in order to identify the considered dynamics in terms of modal damping, natural frequencies and mode shapes. If the system is characterized by time-dependent dynamic properties, the analysis can be carried out by splitting the whole observation time into N_I sub-intervals I_i, $i = 1, ..., N_I$, where the system dynamical features can be considered constant in time. In the considered cases the varying parameter is the natural frequency f_n, thus, an accuracy criterion is defined considering such dynamical property.

From the identification point of view, the estimated natural frequency is achieved within an accuracy given by the frequency resolution Δf_n (numerical error and round-off errors are not considered) which is, in turn, related to the length of the time-interval where the dynamics is observed. In the same time interval, if the natural frequency is varying in time, one can assume that $f_n = \check{f}_n + \Delta_{obs} f_n$ where $\Delta_{obs} f_n$ represents the time variation of the natural frequency, in the considered interval, with respect to a reference value $\check{f}_n$. Without loss of generality, it can be assumed that $f_n = \check{f}_n$.

In order to consider the system properties constant over the generic interval I_i it is necessary that the variation of the natural frequency in time is less or equal to the frequency resolution. In this case the physical quantity that has to be estimated has no observable variation. Thus, the following condition must hold:

$$\Delta_{obs} f_n \leq \Delta f_n \tag{15}$$

The variation in time can be defined as

$$\Delta_{obs} f_n = \dot{f}_n \Delta t \tag{16}$$

where

$$\dot{f}_n = max_I \left[\dot{f}(t) \right] \qquad t \in [t_I, t_I + \Delta t]$$

By recalling that the frequency resolution is $\Delta f_n = 1/\Delta t$ and by using Eq. 16, the condition given by Eq. 15 become:

$$\dot{f}_n \Delta t \leq 1/\Delta t \tag{17}$$

Therefore, an estimate of the length of the observation time-window is given, see Eq. 17, by:

$$\Delta t \leq \sqrt{\frac{1}{\dot{f}_n}} \tag{18}$$

Equation 18 shows that the faster the rate of variation of f_n is, the smaller the length of the observation interval must be in order to apply the OMA techniques to an almost time-independent system (in the given observation time-window). From the practical point of view the criterion introduced in Eq. 18 affects the accuracy of the modal parameter estimates and limits the applicability of the OMA methods when dealing with time-dependent systems. Indeed, not only the maximum frequency resolution depends on the rate of variation of natural frequency but also on the number of samples available for OMA, that is $\Delta t = N_s \Delta_s t$ where $\Delta_s t$ is the given sampling time. By reducing the available number of samples also the numerical error associated to the identification procedure increases. Therefore, such an operative criterion of applicability of the OMA techniques applied to time-dependent systems links the accuracy of the estimates to the rate of variation of the unknown system characteristics, namely the higher the rate of variation is the lower the accuracy of the estimate is.

4 Analysis of flight data

The considered data refer to different flight conditions of a Launch Vehicle. Such conditions consider different excitation loading and different modal parameters to be estimated. These data sets, which are adimensionalized with respect to reference values intentionally left unknown, are organized in two different cases: Case 1 and Case 2 representing two different phases of the flight.

4.1 Case 1

In Case 1 the dynamic response is measured by three accelerometers whose locations are intentionally left unknown. Specifically, the time-frequency response is obtained by evaluating the PSD with a suitable time-window. The input nature is unknown and it is assumed to be white noise at least in the bandwidth of interest.

It can be observed that there are two target modes around 20 Hz and 40 Hz. The damping is expected to be in around the interval $0.20\% - 2.00\%$. The provided data are considered synchronous and analyzed in the interval $[10s - 100s]$. The Nyquist frequency is 227.27 Hz. In Figure 1 the analyzed time-histories are reported.

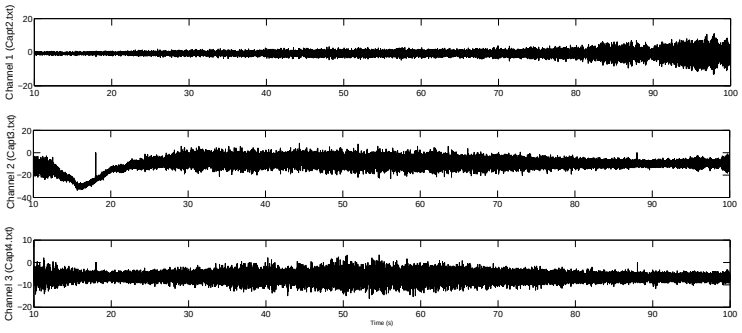

Fig. 1: Analyzed time-histories

In order to track the change of modal parameters over time, a trade-off has been made between the frequency variation (at least supposed to be) and the time duration of the analysis time-window. Because it is expected a frequency variation of about 0.1 Hz/s then, see Sec. 3, a frequency resolution of at 0.1 Hz is assumed to be correct to follow the dynamic of the studied system. Thus, a time observation window of $10s$ will be used for every analysis.

4.1.1 Frequency Domain Decomposition Analysis

In the performed analysis the Nyquist Frequency is 227.27 Hz and all the interval analysis I_i, $i = 1, ..., 10$ are of 10s length. Moreover, the FDD is performed with a Theshold MAC of 0.90. The Figure 1, shows a strongly time-dependent non-zero mean value up to $30s$, thus violating the OMA-hypotheses. The analyses in the first two time windows *i.e.*, $I_1 = [10s, 20s]$ and $I_1 = [20s, 30s]$, have been performed considering first all the three channels then only channel 1 and channel 3 in order to evaluate the effects on the estimates

of such type of data. It is relevant to point out that for all the channels the mean value on the generic I_i is filtered out before the analysis.

The estimated natural frequencies f_n obtained using the FDD approach are shown in Figs. 2 and 3, for the two modes respectively, where some interpolating lines of different orders are also drown in order to give a better idea of the time-dependency of the results. In particular, the two identified natural

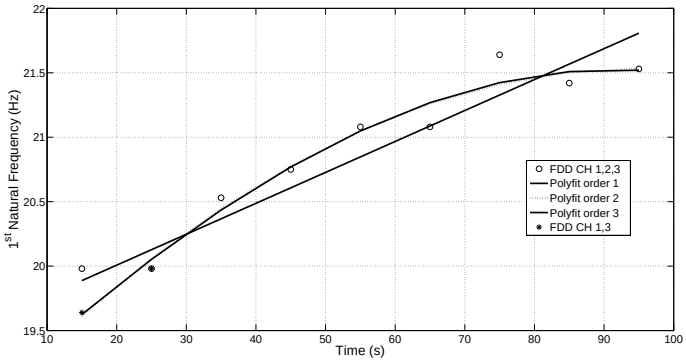

Fig. 2: Time dependence of first natural frequency

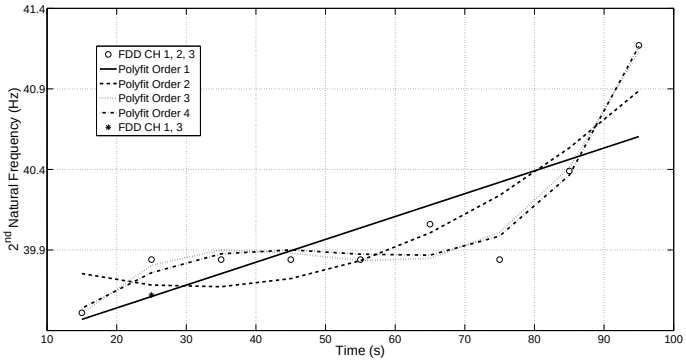

Fig. 3: Time dependence of second natural frequency

frequency are in the ranges $f_{n_1} \in [19.81, 21.64]Hz$, $f_{n_2} \in [39.57, 41.04]Hz$. Moreover, it has been observed that by using only Channel 1 and 3 in $[10s, 20s]$ in order to avoid the effect of the time-varying mean valued of Channel 2 does not permit the identification of the second natural frequency. Thus, in the next analyses all the channel will be considered.

The estimated damping ratios ζ_n are shown in Fig. 4 together with the associated regression lines. Globally, Figure 4 shows that the estimated damp-

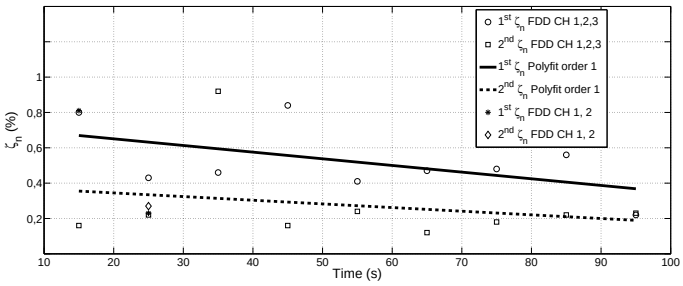

Fig. 4: Identified damping ratios, Threshold MAC=0.9

ing ratios are in the intervals $\zeta_1 \in [0.22\%, 0.84\%]$, $\zeta_2 \in [0.16\%, 0.22\%]$ with average damping coefficients: $\bar{\zeta}_1 = 0.52\%$, $\bar{\zeta}_2 = 0.27\%$ and associated standard deviations on the whole time-window of $\sigma_{\zeta_1} = 0.19\%$, $\sigma_{\zeta_2} = 0.25\%$.

Finally, in order to evaluate the time-evolution of the mode shapes, all the modes in the different time interval of analysis are compared, by using the MAC where the reference modes are chosen those evaluated in the $I_1 = [10s, 20s]$ time-intervals. The results are shown in Fig. 5 where both the two identified modes show a significant variation at the end of the considered time-window,*i.e.*, in the interval $[70s, 100s]$.

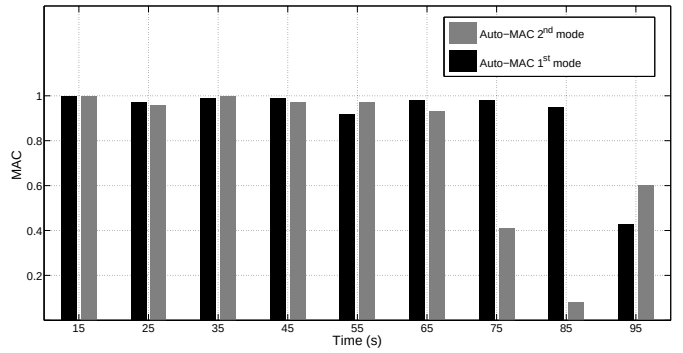

Fig. 5: Identified Modes variation

4.1.2 Hilbert Transform Method Analysis

In the performed analysis the Nyquist Frequency is 227.27 Hz and all the interval of analysis I_i, $i = 1, ..., 10$ are of 10s length. All the channels have been used for all the analyses and for all the channels the mean value on the generic I_i is filtered out before the analysis starts. The estimated natural frequencies f_n obtained using the HTM are shown in Figs. 6 and 7 where some interpolating lines of different orders are drown in order to give an idea of the time-dependency of the results.

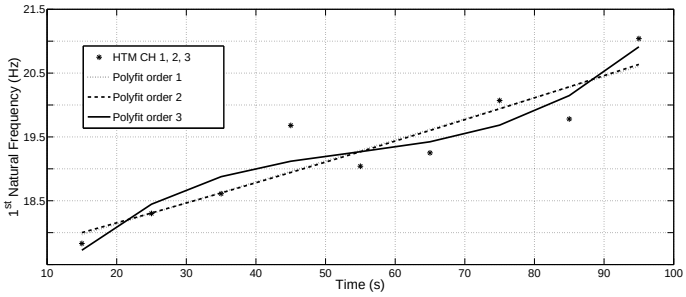

Fig. 6: Time dependence of first natural frequency

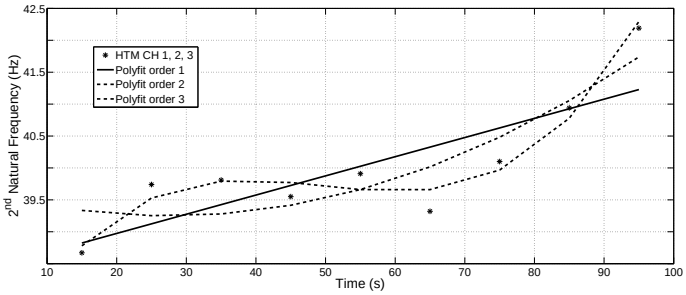

Fig. 7: Time dependence of second natural frequency

In particular, it has been obtained that the natural frequencies vary in the ranges $f_{n_1} \in [17.83, 21.04]Hz$, $f_{n_2} \in [38.67, 42.19]Hz$. The estimated damping ratios ζ_n using the HTM approach are shown in Fig. 8 in which also the associated regression lines are drown. From Figure 8 one can observe that the estimated damping ratios are in the intervals $\zeta_1 \in [0.30\%, 2.16\%]$, $\zeta_2 \in [0.35\%, 1.67\%]$. Moreover, on the whole observation window the average damping ratios are $\bar{\zeta}_1 = 1.10\%$, $\bar{\zeta}_2 = 0.89\%$ with a standard deviation damping $\sigma_{\zeta_1} = 0.68\%$, $\sigma_{\zeta_2} = 0.38\%$

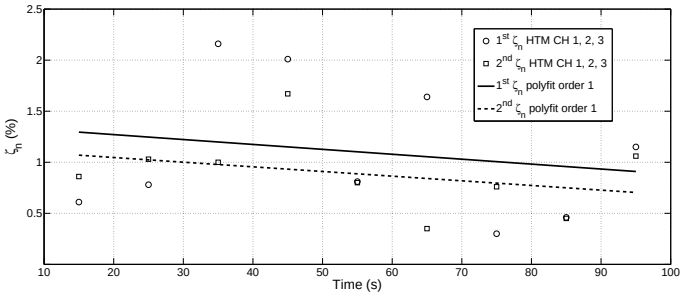

Fig. 8: Identified damping ratios, Threshold MAC=0.9

The mode shapes evolution has been evaluated by comparing via the MAC those evaluated in the generic time-interval I_i with those identified in $I_1 = [10s, 20s]$. The results are shown in Fig. 9 where both modes show a significant

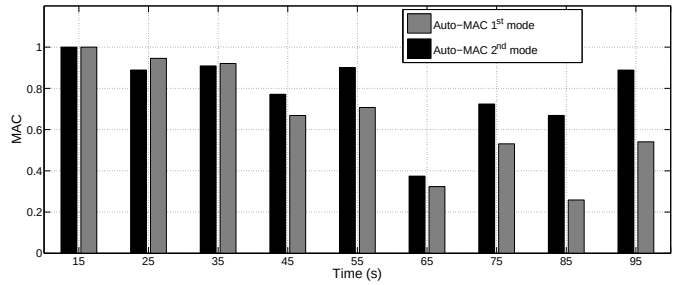

Fig. 9: Identified Modes variation

variation at the end of the considered time-window, *i.e.*, $[60s, 100s]$: a result similar to the one obtained via FDD.

4.1.3 Comparison between FDD and HTM

In this Section the results obtained via FDD and HTM are compared in order to enforce the results obtained by the two methods. From Figures. 5 and 9 it appears that the two different methods have a similar behavior for both the identified modal shapes although the modes exhibit by HTM show a larger variation. Moreover, by considering the damping ratios, see Figs. 4 and 8, a similar trend of identified ζ_n is shown. Specifically, the damping ratios estimated with HTM approach are slightly higher with respect to those identified using the FDD method. However, by considering the standard deviation and the average value of the ζ_n time-distribution, the two results fall in the same interval of magnitude. A comparison between the frequencies identified by HTM

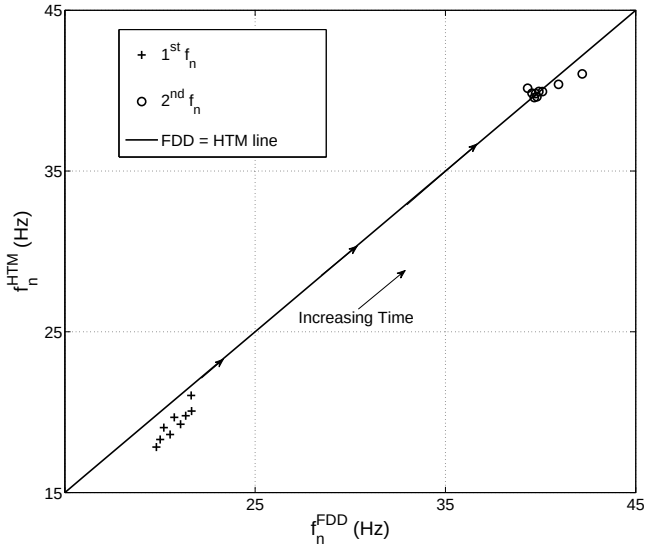

Fig. 10: Identified Modes variation

and FDD is shown in Fig. 10. Figure 10 shows that all the results obtained via FDD and HTM differ for less than 2 Hz. It is important to underline that because of it is not present a reference value for the estimated frequency the comparison between two OMA methods provides also an indirect evaluation of the consistency of obtained results. This approach will be followed also in the next Section where the same procedure is not only applied between two different OMA methods but also to different data sets referring to the same flight condition.

4.2 Case 2

The second case corresponds to a flight phase where the system is excited by a supposed white noise and the responses are recorded in correspondence of 4 locations left intentionally unknown. The only available information on the systems is that the target modes are vibrating with natural frequencies located around at 10-20 Hz and 30-40 Hz. No information are available concerning about the values of damping ratios. The data are considered synchronous and analyzed in the time interval $200s - 500s$ and sampled with a Nyquist Frequency of 227.27 Hz. Three data sets with the same sampling rate are available: Flight1, Flight2 and Flight3. In Figure 11 the analyzed time-history are reported together with the excitation for the data set named Flight 1, as an example. In order to follow the change of modal properties over time, a trade-off between the frequency variation (at least supposed to be) and time

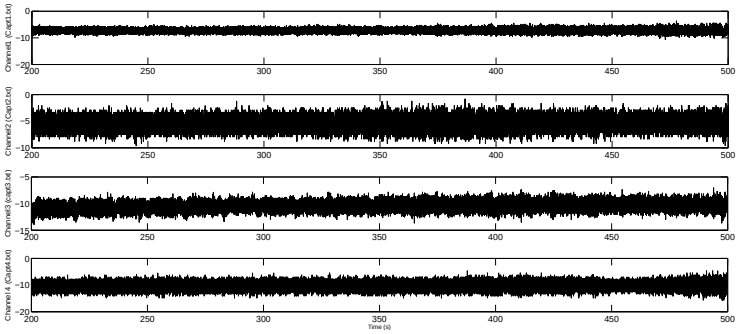

Fig. 11: Recorded excitation and channels time histories for the Flight1 data set

duration of the analysis time-windows has been carried out. Thus, any analysis has been performed on a time-window of $10s$.

4.2.1 Frequency Domain Decomposition analysis

In the performed analysis the Nyquist Frequency is 227.27 Hz. The analysis will be performed in interval of analysis I_i, $i = 1, ..., 10$ of length of 10s. Moreover, the FDD is performed with a Threshold MAC of 0.90. Moreover, for all the channels the mean value on the generic I_i is filtered out before the analysis.

By applying the FDD approach, three natural frequencies are estimated for Flight1, see Figs. 12, 13 and 14 the three natural frequencies identified for the Flight1 case are shown, respectively.

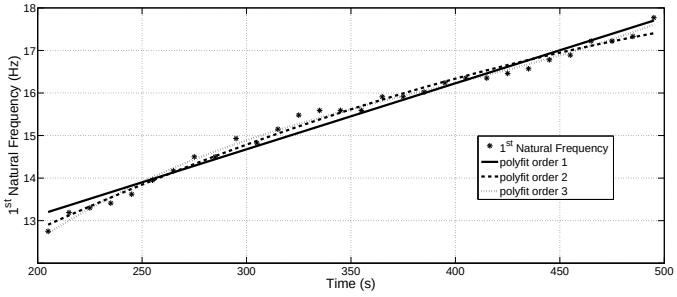

Fig. 12: Time dependence of first natural frequency, Flight1

In particular, f_{n_2} is not identified in $[260s, 270s]$ and the global interval of variation of the natural frequency are $f_{n_1} \in [12.75, 17.77]Hz$, $f_{n_2} \in$

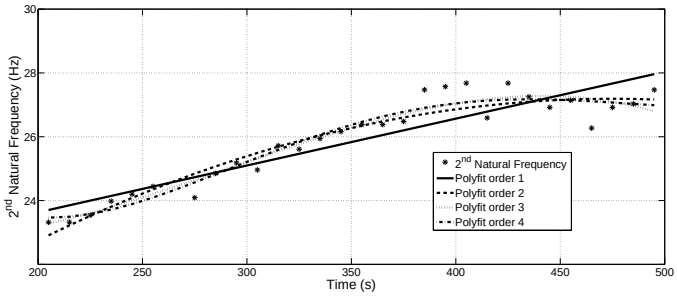

Fig. 13: Time dependence of second natural frequency, Flight1

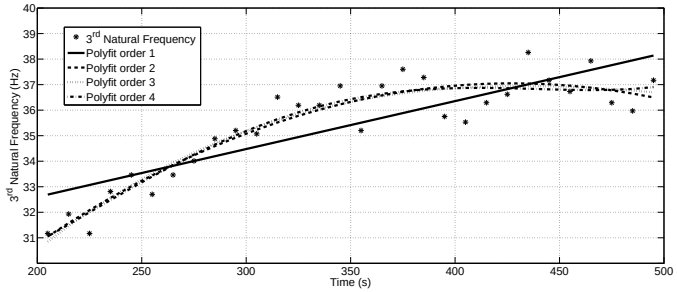

Fig. 14: Time dependence of third natural frequency, Flight1

$[23.32, 27.47]Hz$ and $f_{n_3} \in [31.17, 37.17]Hz$. The same number of natural frequencies has been estimated considering the Flight2 data, as reported in Figs. 15, 16 and 17. Specifically, the estimated interval of variation of the natural frequency of the Flight2 case are
$f_{n_1} \in [12.82, 17.66]Hz$, $f_{n_2} \in [23.26, 29.26]Hz$, $f_{n_3} \in [32.49, 38.95]Hz$. Moreover, as for Flight1, the second natural frequency f_{n_2} is not identified in $[260s, 270s]$. Finally, as for Flight1 and Flight2, also for the Flight3 data

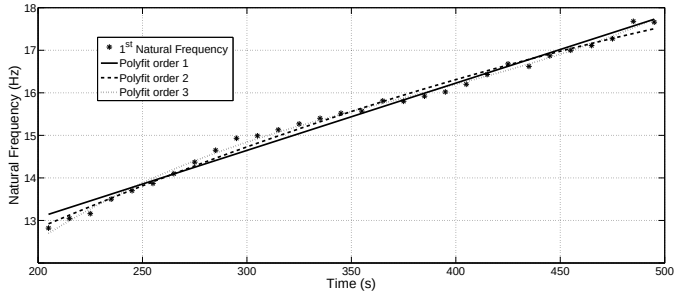

Fig. 15: Time dependence of first natural frequency, Flight2

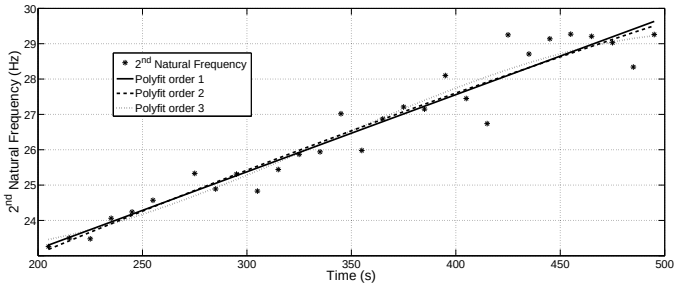

Fig. 16: Time dependence of second natural frequency, Flight2

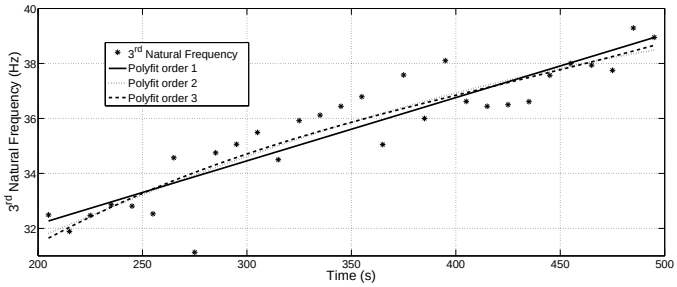

Fig. 17: Time dependence of third natural frequency, Flight2

sets three natural frequencies have been identified, see Figs. 18, 19 and 20. The depicted results show that for the Flight3 data set all the natural fre-

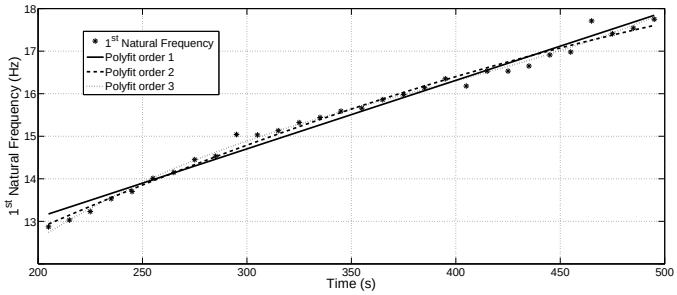

Fig. 18: Time dependence of first natural frequency, Flight3

quencies have been estimated in all the time intervals. Moreover, the estimated

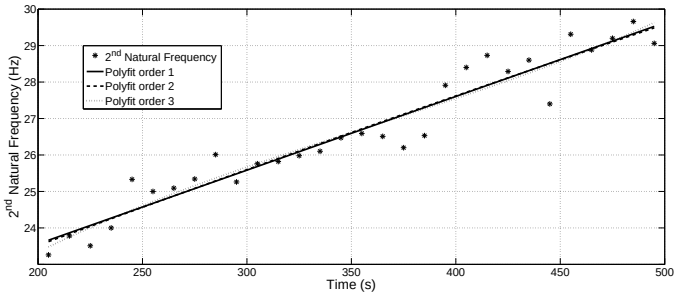

Fig. 19: Time dependence of second natural frequency, Flight3

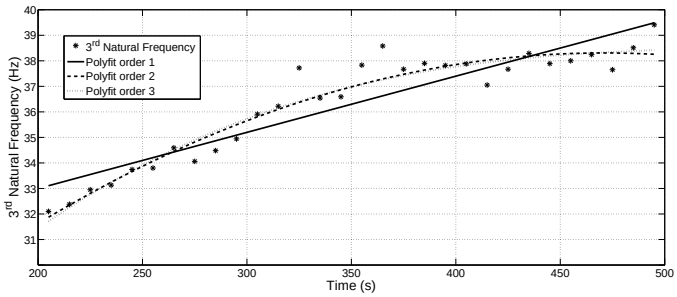

Fig. 20: Time dependence of third natural frequency, Flight3

intervals of variation are $f_{n_1} \in [12.87, 17.75]Hz,\ f_{n_2} \in [23.26, 29.06]Hz,\ f_{n_3} \in [32.10, 39.41]Hz$.

The obtained results show a consistency of the identified natural frequencies using the FDD approach with all the three different data sets (corresponding to the three flights), but only by using the Flight3 data set all the frequencies have been identified for all the time-intervals considered. Figures 21 shows a direct comparison of the natural frequencies identified in all the three considered flights which permits to appreciate the robustness of frequency identification of FDD.

The estimated damping ratios ζ_n using the FDD approach are shown in Fig. 22 where also the associated regression lines are drown. The damping ratios estimated for Flight1 vary in the following intervals $\zeta_1 \in [0.46\%, 0.89\%],\ \zeta_2 \in [0.19\%, 0.40\%],\ \zeta_3 \in [0.13\%, 0.55\%]$ and from a global point of view are characterized by average values on the whole time observation window of $\bar{\zeta_1} = 0.67\%$, $\bar{\zeta_2} = 0.27\%$, $\bar{\zeta_3} = 0.24\%$ with associated standard deviation of $\sigma_{\zeta_1} = 0.14\%$, $\sigma_{\zeta_2} = 0.08\%$, $\sigma_{\zeta_3} = 0.09\%$.

In Figure 23 the identified damping ratios for the Flight2 data set are shown. The damping ratios estimated for Flight2 vary in the following intervals $\zeta_1 \in [0.55\%, 1.60\%],\ \zeta_2 \in [0.16\%, 0.54\%],\ \zeta_3 \in [0.13\%, 0.46\%]$ and from a global point of view are characterized by average values on the whole time

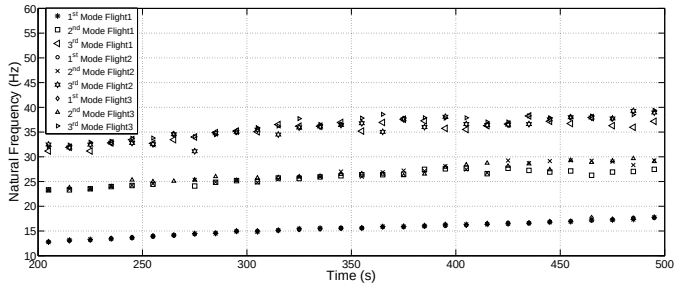

Fig. 21: Comparison of the natural frequency for different flights

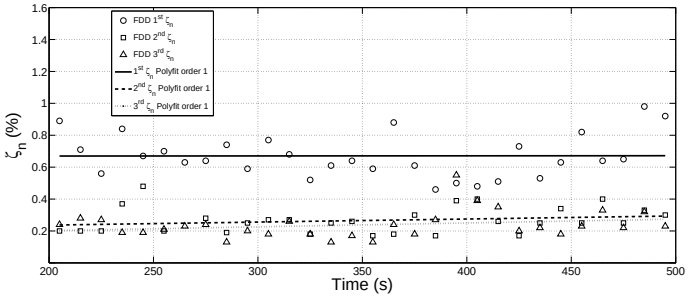

Fig. 22: Identified damping ratios Flight1, Threshold MAC=0.9

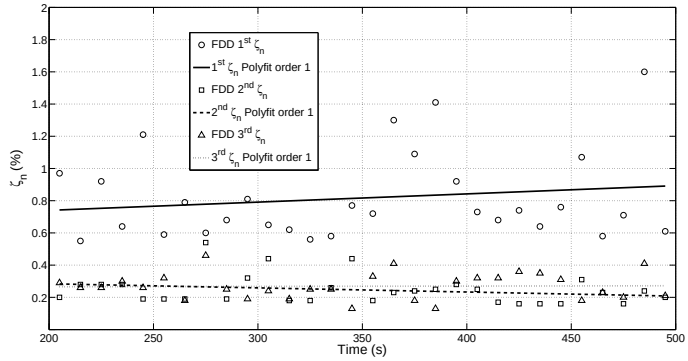

Fig. 23: Identified damping ratios Flight2, Threshold MAC=0.9

observation window of $\bar{\zeta_1} = 0.82\%$, $\bar{\zeta_2} = 0.25\%$, $\bar{\zeta_3} = 0.27\%$ with an associated standard deviation of $\sigma_{\zeta_1} = 0.05\%$, $\sigma_{\zeta_2} = 0.02\%$, $\sigma_{\zeta_3} = 0.00\%$. Observe that even if the standard deviation $\sigma_{\zeta_3} = 0.00\%$ this does not means that the estimated coefficient does not deviate from the mean valued in the analysis intervals but it means that ζ_3 does not deviate up to the second digit.

Finally, in Figures 24 the damping ratios for the Flight3 data set are shown. The identified damping ratios vary in the intervals $\zeta_1 \in [0.44\%, 1.71\%]$, $\zeta_2 \in$

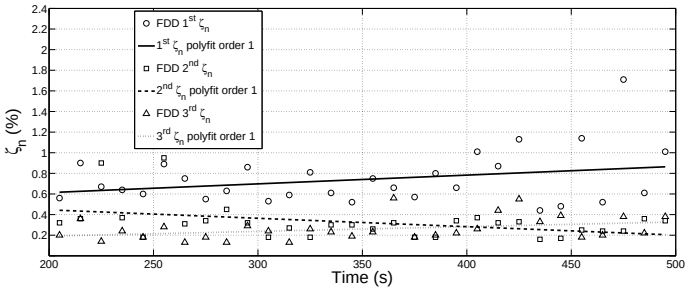

Fig. 24: Identified damping ratios, Threshold MAC=0.9

$[0.16\%, 0.95\%]$, $\zeta_3 \in [0.14\%, 0.56\%]$ and from a global point of view are characterized by average values on the whole time observation window of $\bar{\zeta_1} = 0.74\%$, $\bar{\zeta_2} = 0.32\%$, $\bar{\zeta_3} = 0.26\%$ with an associated standard deviation of $\sigma_{\zeta_1} = 0.25\%$, $\sigma_{\zeta_2} = 0.18\%$, $\sigma_{\zeta_3} = 0.11\%$.

It is worth to note that by observing all the average values for all the data sets and their associated time standard deviations together with their interval of variation one can conclude that the identified quantities are similar for all the considered flights. As for the frequencies in Flight1 and Flight2 in the interval $[200s, 210s]$, the second mode damping ratio has been not identified.

In order to evaluate the natural mode shapes evolution, all the identified modes in the different intervals of analysis have been compared via the Modal Assurance Criterion where the reference mode is the one identified in $I_1 = [10s, 20s]$. The results are shown in Fig. 25 for all the Flight1 data set, in Fig. 26 for the Flight2 data set and in Fig. 27 for the Flight3 data set.

For all the different data sets analyzed, the first mode is the one identified with the best accuracy and it shows a slow variation in the considered time-intervals. As for the natural frequencies in Flight1 and Flight2 for the interval $[200s, 210s]$, the second mode is not identified because it is not possible to identify the corresponding f_n due to too many uncertainties in the time-histories. Indeed, the singular values distribution around those frequencies exhibited several local maxima but none of them was much higher then the other ones, thus not providing a clear information on the natural frequency.

4.2.2 Hilbert Transform Method Analysis

In the performed analysis the Nyquist Frequency is 227.27 Hz and all the interval of analysis I_i, $i = 1, ..., 10$ are of 10s length. In all the channels the mean value on the generic I_i is filtered out before the analysis.

For the Flight1 data sets three natural frequencies have been identified, see Figs. 28, 29 and 30. All the target f_n for all the considered time-interval have

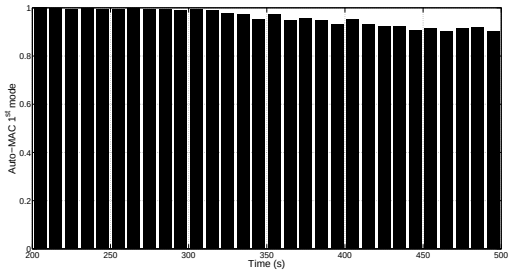

(a) First identified mode

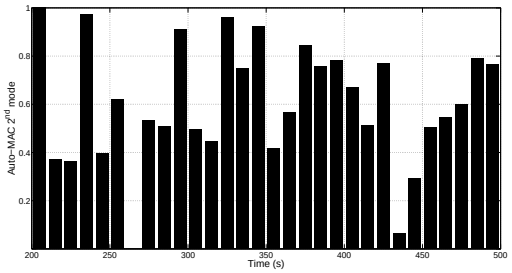

(b) Second identified mode

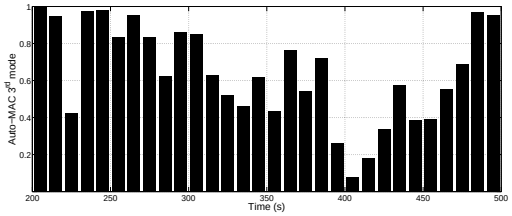

(c) Third identified mode

Fig. 25: Flight1: identified Modes variation

been identified by considering the Flight1 data set and $f_{n_1} \in [13.16, 17.85]Hz,\ f_{n_2} \in [22.77, 28.93]Hz,\ f_{n_3} \in [31.01, 39.00]Hz$.

In Figures 31, 32 and 33 the three natural frequencies identified for the Flight2 case are shown. In particular, it has been obtained that $f_{n_1} \in [12.73, 17.27]Hz,\ f_{n_2} \in [22.63, 29.25]Hz,\ f_{n_3} \in [31.17, 39.12]Hz$ Finally, also for Flight3 data set three natural frequencies have been identified, see Figs. 34, 35 and 36. The identified interval of variation of the natural frequencies are $f_{n_1} \in [12.90, 17.78]Hz,\ f_{n_2} \in [22.43, 29.27]Hz,\ f_{n_3} \in [30.67, 39.50]Hz$.

For all the given data sets the natural frequencies identified in all the time intervals using the HTM approach are congruent with themselves. Figure 37

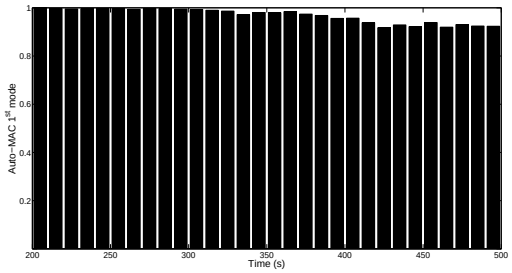

(a) First identified mode

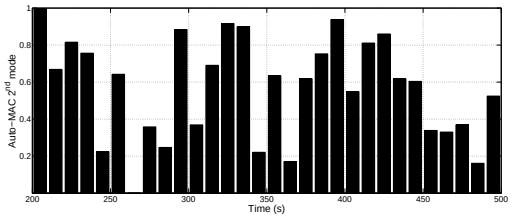

(b) Second identified mode

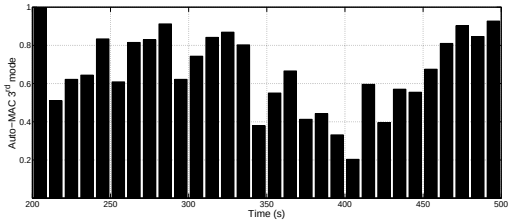

(c) Third identified mode

Fig. 26: Flight2: identified Modes variation

shows a direct comparison of the natural frequencies identified in all the three considered flights, thus confirming the consistency of the results.

The identified damping ratios for the Flight1 data set are shown in Fig.38. The estimated damping ratios vary in the intervals $\zeta_1 \in [0.21\%, 2.01\%]$, $\zeta_2 \in [0.10\%, 2.45\%]$, $\zeta_3 \in [0.18\%, 2.00\%]$ with an average on the whole observation time window of $\bar{\zeta}_1 = 0.93\%$, $\bar{\zeta}_2 = 0.88\%$, $\bar{\zeta}_3 = 0.86\%$ with the associated time standard deviation damping coefficients: $\sigma_{\zeta_1} = 0.52\%$, $\sigma_{\zeta_2} = 0.62\%$, $\sigma_{\zeta_3} = 0.52\%$.

In Figure 39 the identified damping ratios for the Flight2 data set are shown. The estimated damping ratios vary in the intervals $\zeta_1 \in [0.11\%, 1.61\%]$, $\zeta_2 \in [0.19\%, 2.03\%]$, $\zeta_3 \in [0.10\%, 2.14\%]$ with an average on the whole observation time window of $\bar{\zeta}_1 = 0.79\%$, $\bar{\zeta}_2 = 0.95\%$, $\bar{\zeta}_3 = 0.80\%$ with the associated time

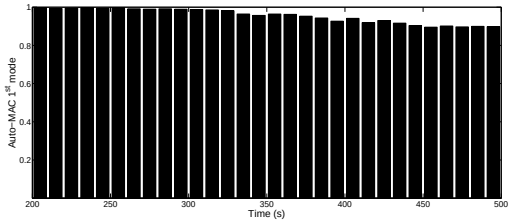

(a) First identified mode

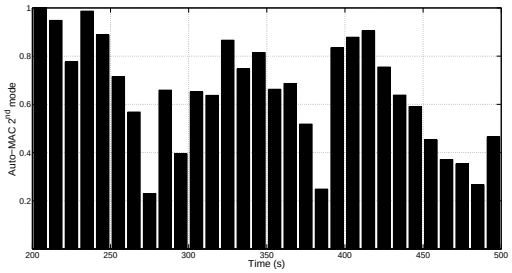

(b) Second identified mode

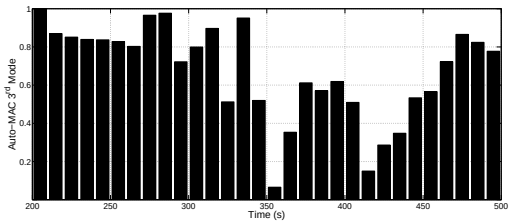

(c) Third identified mode

Fig. 27: Flight2: identified Modes variation

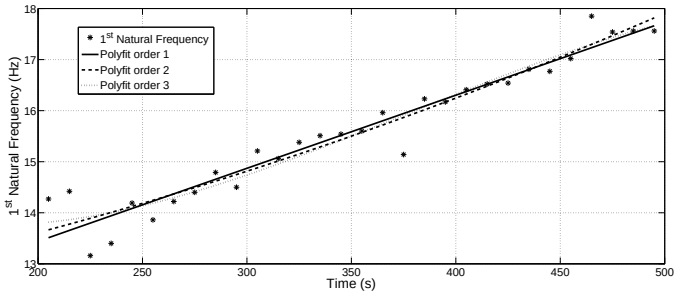

Fig. 28: Time dependence of first natural frequency

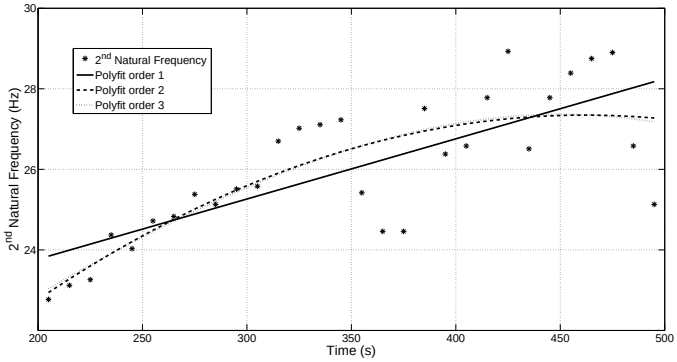

Fig. 29: Time dependence of second natural frequency

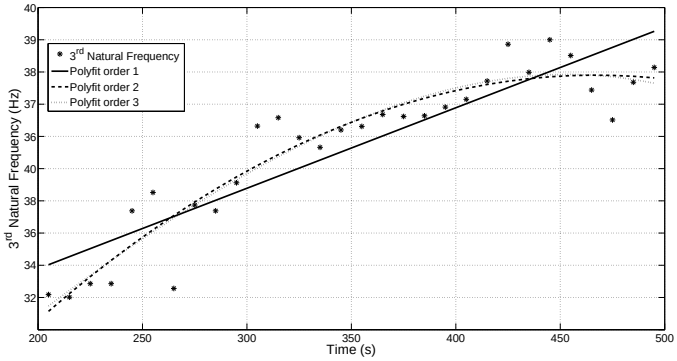

Fig. 30: Time dependence of third natural frequency

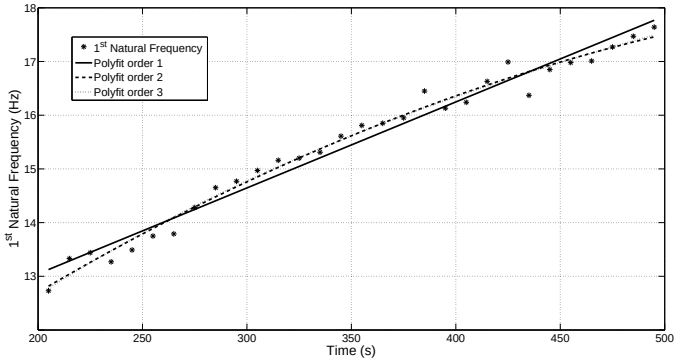

Fig. 31: Time dependence of first natural frequency

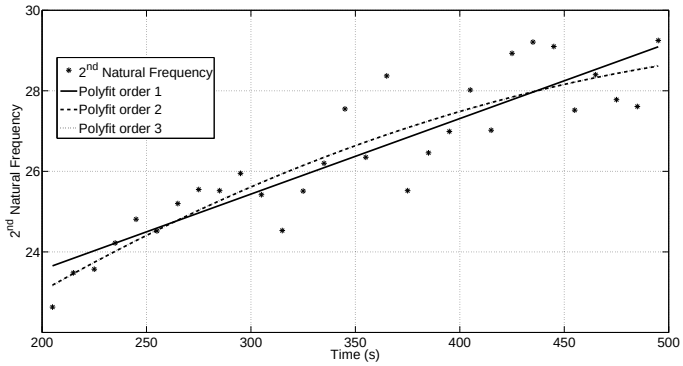

Fig. 32: Time dependence of second natural frequency

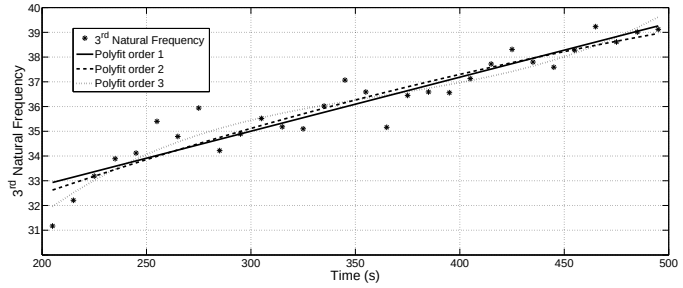

Fig. 33: Time dependence of second natural frequency

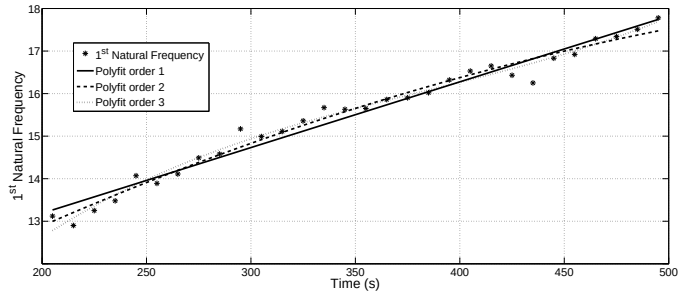

Fig. 34: Time dependence of first natural frequency

standard deviation damping coefficients: $\sigma_{\zeta_1} = 0.43\%$, $\sigma_{\zeta_2} = 0.52\%$, $\sigma_{\zeta_3} = 0.60\%$.

In Figures 40 the identified damping ratios for the Flight3 data set are reported. The estimated damping ratios vary in the intervals $\zeta_1 \in [0.15\%, 1.34\%]$ $\zeta_2 \in [0.11\%, 2.61\%]$, $\zeta_3 \in [0.16\%, 1.93\%]$ with an average on the whole obser-

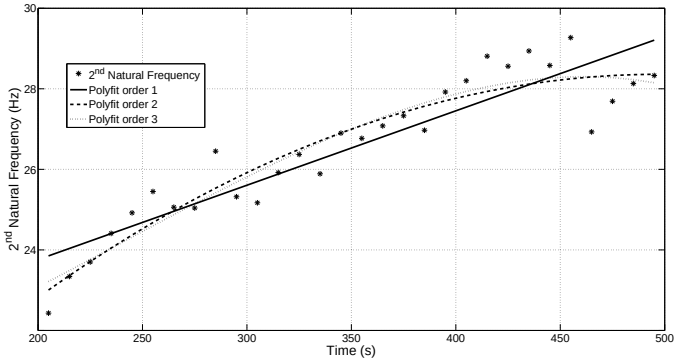

Fig. 35: Time dependence of second natural frequency

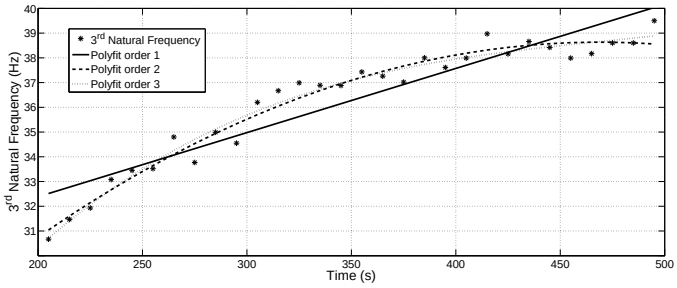

Fig. 36: Time dependence of second natural frequency

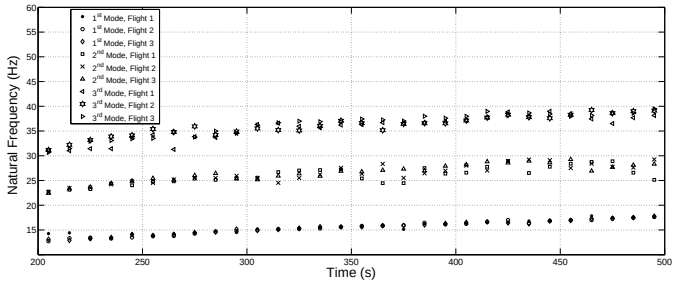

Fig. 37: Comparison of the natural frequency for different flights

vation time window of $\bar{\zeta_1} = 0.67\%$, $\bar{\zeta_2} = 0.93\%$, $\bar{\zeta_3} = 0.72\%$ with the associated time standard deviation damping coefficients: $\sigma_{\zeta_1} = 0.37\%$, $\sigma_{\zeta_2} = 0.65\%$, $\sigma_{\zeta_3} = 0.53\%$.

By comparing all the average values for all the data sets and their time standard deviation together with their interval of variation it appears that the identified damping properties are very similar for all the flights.

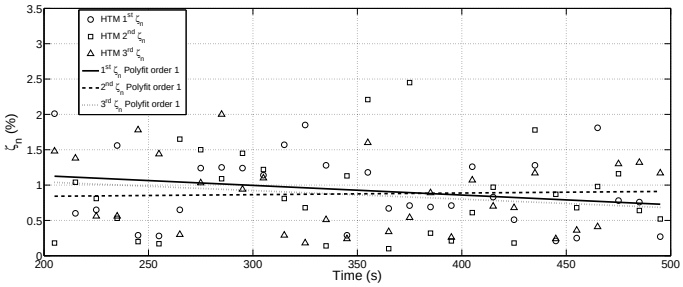

Fig. 38: Identified damping ratios Flight1

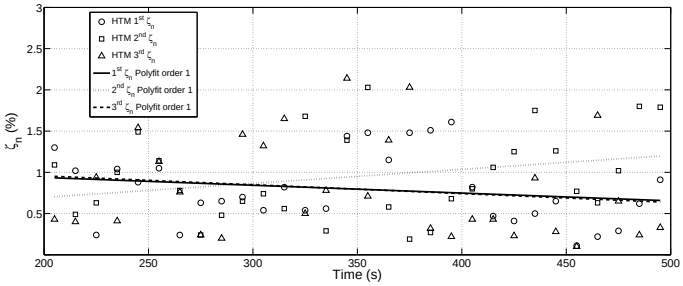

Fig. 39: Identified damping ratios Flight2

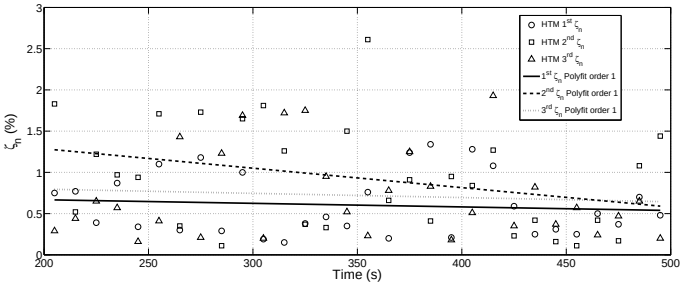

Fig. 40: Identified damping ratios Flight3

In order to evaluate the mode shape evolution all the modes in the different interval of analysis have been compared via the Modal Assurance Criterion with the corresponding mode identified in $I_1 = [10s, 20s]$. The results are shown in Fig. 41 for the Flight1 data set, in Fig. 42 for the Flight2 data set and Fig. 43 for the Flight3 data set.

For all the different data sets the first mode is the one better identified and it shows a slow variation on the considered time interval as for the FDD identification. Again, the identification of the second and third modes is dif-

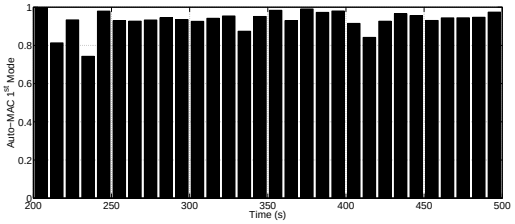

(a) First identified mode

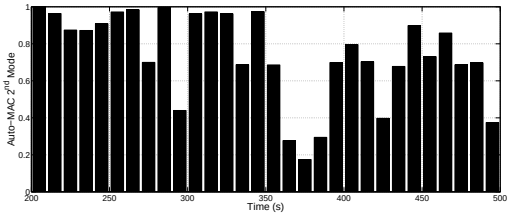

(b) Second identified mode

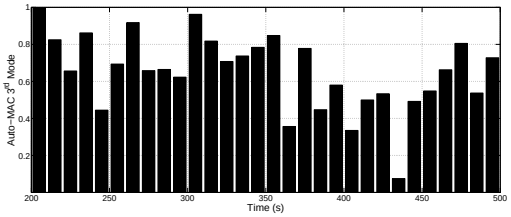

(c) Third identified mode

Fig. 41: Flight2: identified Modes variation

ficult due to the small number of spatial measure point available and limited sampling.

4.2.3 Comparison between FDD and HTM

A comparison between the natural frequencies identified by HTM and FDD, for all the considered Flight data, is shown in Fig. 44. This Figure shows that all the results obtained via FDD and HTM have a maximum difference of about $5Hz$. By considering the damping ratios, a similar trend (not reported) is obtained for all the flights but HTM gives a higher damping values with respect to FDD (about 1%). The mode time-variations are similar for all the considered flights. Specifically, the first mode slowly changing in time and well identified. Otherwise, the second and the third modes appear to experience a greater variation during the considered flight phases due to both the intrinsic

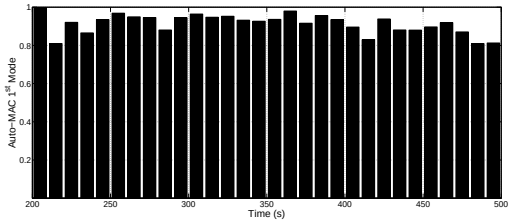

(a) First identified mode

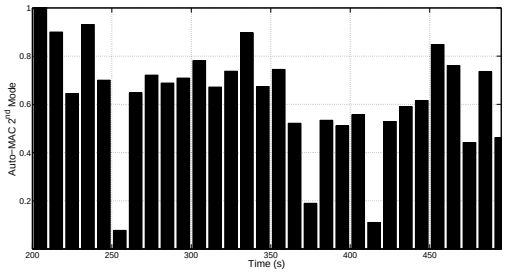

(b) Second identified mode

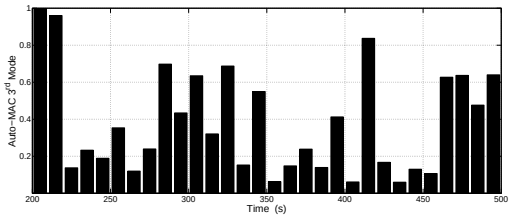

(c) Third identified mode

Fig. 42: Flight2: identified Modes variation

nature of the system properties and the reduced number of measurement points together with the higher corresponding natural frequency.

5 Discussion on the accuracy of the estimates

From the analyses carried out, it can be observed that all the considered OMA techniques are able to identify the target natural frequency f_n. On the contrary, from the damping ratio point of view, the accuracy of the estimates seems to largely vary with the used method and on the particular analyzed case. Starting from this, the evaluation of the accuracy of the estimates seems difficult to asses. However, a bounded accuracy in the natural frequency estimates is clearly identified, whereas the damping ratios have not such bounding

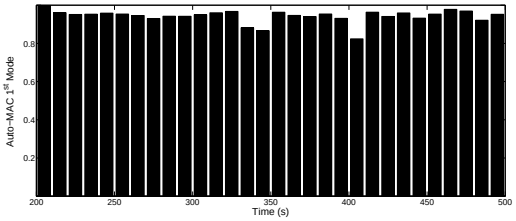

(a) First identified mode

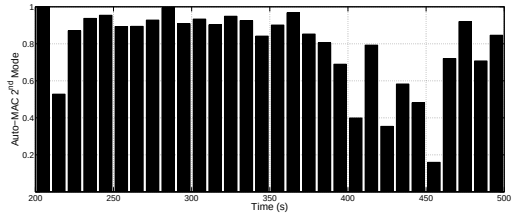

(b) Second identified mode

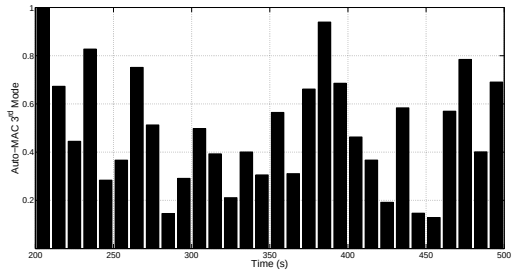

(c) Third identified mode

Fig. 43: Flight2: identified Modes variation

limits for accuracy. The problem of large variations in the estimates of damping coefficient is well-known in literature and in Ref. [15] it is argued from the analytical point of view. Otherwise, in the present paper a different approach is considered by changing the point of view with respect to the system dynamics identification. Thus, the quantities largely used in structural analysis are f_n and ζ_n but, really, the dynamics of the system is characterized by its poles λ_n which are related to the natural frequencies and damping ratios, see Eqs. 19.

$$\begin{aligned} \lambda_n &= \lambda_{R_n} + j\lambda_{I_n} \\ \zeta_n &:= -\frac{\lambda_{R_n}}{\lambda_{I_n}} \\ \lambda_{n_I} &:= \omega_n = 2\pi f_n \end{aligned} \tag{19}$$

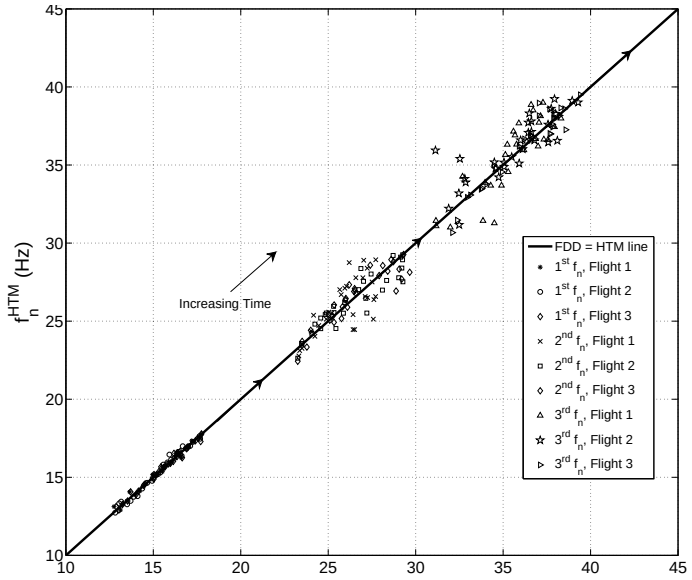

Fig. 44: Comparison of the natural frequency for different flights

Moreover, the system pole (and thus, its dynamics) could be identified by its module and phase:

$$|\lambda_n| = \omega_n \sqrt{1+\zeta_n^2} \tag{20}$$

$$\angle\lambda_n = \frac{\pi}{2} + \text{arctang}(-\frac{\lambda_{R_n}}{\lambda_{I_n}}) = \frac{\pi}{2} + \text{arctang}(\zeta_n) \tag{21}$$

Equations 20 and 21 can be approximated for the usual values of the damping ratios as:

$$|\lambda_n| \cong \omega_n \tag{22}$$

$$\angle\lambda_n \cong \frac{\pi}{2} + \zeta_n \tag{23}$$

By introducing the accuracy of the estimate of the natural frequency, Δf_n, and damping ratio, $\Delta\zeta_n$, and recalling Eqs. 20-21, the accuracy of the overall dynamics could be written, referring to the analyzed cases, as:

$$\Delta|\lambda_n| \cong \Delta\omega_n = 2\pi\Delta f_n = O(1) \tag{24}$$

$$\Delta\angle\lambda_n \cong \Delta\zeta_n = O(10^{-2}) \tag{25}$$

From Eq. 25 follows that even in presence of uncertainties associated to the damping ratio of the same order of magnitude of the identified quantity it will be the uncertainties associated to the natural frequency identification (see Eq. 24) to the define the accuracy of the pole estimation and, thus of the

system dynamics. From Sec. 3 it has been shown that the accuracy of the method, not considering numerical error and round-off errors, can be identified with the frequency resolution and thus, the above results permit to obtain a first accuracy estimate of the obtained results. Moreover, it is worth to note that Eq. 24 implies that for a fixed sampling time, the greater the frequency variation velocity the higher the uncertainties associated to the identification process. That is the accuracy of the estimate is driven by the accuracy of the estimate of the natural frequency. The above observations on the system poles identification permit to evaluate the accuracy of the different OMA techniques if the exact value of the natural frequency to be estimated is known.

6 Conclusions

Two different OMA methodologies have been used in order to identify the dynamic properties of a launch vehicle in terms of natural frequencies, mode shape variations and damping ratios, considering its actual operative conditions. The first used method is the Frequency Domain Decomposition whereas the second one is the Hilbert Transform Method. Both methods provide estimates for the modal parameters which are in agreement with the declared target modes. Because of the few information available a direct evaluation of the estimate has been not possible otherwise, this issues has been addressed by defining a criterion of practical applicability of OMA techniques to systems with time-varying dynamical properties. This criterion links the physical variation of modal parameters to the time-observation-window by permitting to reduce the physical uncertainty to the frequency resolution. Moreover, it has been demonstrated, by arguing from system theory, that the driving uncertainty in the dynamical identification is the one associated with the natural frequency which *de facto* identify the position of the system poles on the complex plane. The obtained results with the two different methods have been compared showing a consistency between the estimates. Moreover, when available, the results obtained with the same method have been compared with those obtained for the same method but associated to different data sets for equal flight conditions. From the point of view of the mode shapes, they have been studied by observing how the identified mode varies from itself evaluated at the beginning of the studied time-window. This have shown similar behavior both in FDD and HTM methods even if more sensors and time samples are required for better estimates of the higher-order modes.

References

1. L. Hermans, H. Van der Auweraer. Industrial Applicability of Modal Analysis on Operating Data. Proceedings NATO Advance Study Institute on Modal Analysis and Testing, 1998, NATO, Seimbra (P).
2. R. Brincker, L. Zhang, P. Andersen. Modal Identification from Ambient Responses Using Frequency Domain Decomposition. Proceedings of XVIII International Modal Analysis Conference, 2000, IMAC, San Antonio, TX(USA).

3. A. Agneni, L. Balis Crema, G. Coppotelli. Time and Frequency Domain Model Parameter Estimation by Output Only Functions. Proceedings of International Forum on Aeroelasticity and Structural Dynamics, 2003, IFASD, Amsterdam (NL).
4. A. Agneni, L. Balis Crema, G. Coppotelli. Analysis of Structures with Closely Spaced Modes. Mechanical Systems and Signal Processing. Special Issue: Operational Modal Analysis, 2010, 24, 1240-1249.
5. L. Hermans, H. Van der Auweraer. Modal Testing and Analysis of Structures under Operational Conditions: Industrial Applications. Mechanical Systems and Signal Processing, 1999, 13, 193-216.
6. E.A. Robinson, M.T. Silva. Digital Signal Processing and Time Series Analysis. Holden-Day, Inc., San Francisco (USA), 1978.
7. P. Van Overschee and B. De Moor. Subspace Identification for Linear Systems. Kluver Academic Publisher, 1996.
8. W. Heylen, S. Lammens, P. SAS. Modal Analysis Theory and Testing. Kluver Academic Publisher, 1994.
9. R. Brincker and C. E. Ventura and P. Andersen. Damping Estimation by Frequency Domain Decomposition. Proceedings of XIX International Modal Analys Conference, 2001, Kissimee, FL (USA).
10. D.J. Ewins. Modal Testing: Theory and Practice. Research Studies Press Ltd., Tauton, Somerset, (England), 1995.
11. M. Basseville, A. Benveniste, M. Goursat, L. Hermans, L. Mevel, H. Van der Auweraer Output-Only Subspace-Based Structural Identification: From Theory to Industrial Testing Practice. ASME Journal of Dynamic Systems, Measurement, and Control, 123(4), 668-676, 2001
12. R. Pintelon, P. Guillaume, J. Schoukens. Uncertainty calculation in modal (operational) analysis. Mechanical Systems and Signal Processing, 21, 2359-2373,2007
13. E. Reynders, R. Pintelon, G. De Roeck. Uncertainty bonds on modal parameters obtained from stochastic subspace identificaiton. Mechanical Systems and Signal Processing, 22, 948-969,2009
14. Au Sk, F.L. Zhang, Ni Y.C.. Bayesian operational modal analysis:theory, computation, practice. Computers and Structures, 126, 3-14,2013
15. Siu-Kui Au. Uncertainty law in ambient modal identification. Part. I: Theory. Mechanical Systems and Signal Processing, 48, 15-33,2014
16. W.J. Larson, J.R. Wertz Space Technology Library, Vol. 8, Springer Netherlands, 1999